Complete solid buckling analysis with Boundary Face Method

Guangyao Li[1], Shuaiping Guo[1], Jianming Zhang[1,2], Baiping Fei[1], Yuan Li[1]

State Key Laboratory of Advanced Design and Manufacturing for Vehicle Body, College of Mechanical and Vehicle Engineering, Hunan University, Changsha 410082, China

---

[2]Corresponding Author:

Jianming Zhang

College of Mechanical and Vehicle Engineering

Hunan University

Changsha, Hunan, 410082

P.R. China

Tel: 86 731 88823061

Fax: 86 731 88822051

Email: zhangjm@hnu.edu.cn

Complete solid buckling analysis with Boundary Face Method

Guangyao Li[1], Shuaiping Guo[1], Jianming Zhang[1,2], Baiping Fei[1], Yuan Li[1]

Abstract: In this paper, we will propose a new concept, namely the Complete Solid Buckling Analysis, in which the deformation assumptions for rods, beams and plates are all discarded, and the entire structure, including all its local small-sized features, is modeled as a three-dimensional (3D) solid according to its real shape and dimensions. Firstly, we derive a new control equation, in which physical variables in three directions are considered. Then, an equivalent Boundary Integral Equation (BIE) is derived from the control equation. In the numerical implementation, the Boundary Face Method is employed, by which analyses can be performed directly on the CAD geometry model. And the Dual Reciprocity Method is used to deal with the domain integrals. Finally, several numerical examples with different geometries and boundary conditions are presented to test our method. Results are in good agreements with the known ones.

Keywords: buckling analysis，boundary face method，dual reciprocity method

1 Introduction

In structural analysis, problems involving stability assessment have become increasingly important with high-strength steel, truss, plate and shell structures widely used in various fields such as aerospace, bridges, shipbuilding, mining, offshore platforms and high-rise buildings, etc. The buckling analyses of these structures have been investigated analytically and experimentally. Analytical solutions of bar, plate and shell buckling based on the classical theory can be found in references (Brush and Almorth, 1975; Timoshenko and Gere, 1961).

In recent years, the boundary element method (BEM) has become a widely used numerical tool to analyze stability problems of structure (Aliabadi, 2001; Brebbia, 1978; Cheng and Cheng, 2005; Long and Atluri, 2002). Manolis et al. (1986) developed a direct boundary element formulation dealing with linear elastic stability analysis of Bernoulli-Euler beams and Kirchhoff thin plates. Syngellakis and Elzein (1994) extended a boundary element solution of the plate buckling to accommodate any combination of loadings and support conditions. Nerantzaki and Katsikadelis (1996) presented a boundary element formulation for buckling of plates with variable thickness. A more general boundary element formulation of elastic plate buckling analysis, which allowed for wide variety of boundary conditions and arbitrary planar shapes, was presented by Lin et al. (1999). In 2005, Purbolaksono and Aliabadi (2005) presented a formulation for shear deformable plates with general boundary conditions and arbitrary planar shapes. Subsequently, Baiz and Aliabadi (2006,

[1] College of Mechanical and Vehicle Enginnering, Hunan University, Changsha, China

[2] Corresponding author. Tel: +86-371-88823061; Fax: +86-731-88822051;
Email: zhangjm@hnu.edu.cn

2007) introduced a boundary only formulation for buckling analysis of shear deformable shallow shells. Sapountzakis and Tsiatas (2008) developed a boundary element formulation for the general flexural-torsional linear buckling analysis of Timoshenko beams of arbitrarily shaped composite cross-section.

In the above methods of buckling analysis, the real structures are usually modeled using beam, rod, plate and shell elements. The simplified computational model is quite different from the original structure topologically and geometrically, and difficult to take into account the small-sized features of the structure, such as the shape of the welding seams, the welding defects etc. However, the structural stability is very sensitive to the geometry and possible defects of the structure. Therefore, in this paper, we will propose a new concept, namely the **Complete Solid Buckling Analysis**, in which the deformation assumptions for rods, beams, plates and shells are all discarded, and the entire structure, including all of its local small-sized features, is modeled as a 3D solid according to its real shape and dimensions. Firstly, a completely new control equation for buckling analysis of elastic solid is derived using Principle of potential energy, which can be used to analyze the buckling of arbitrary shape structures. Secondly, using the Kelvin fundamental solutions and the Betti's reciprocal theorem, an equivalent BIE is derived from the new control equation. In recent years, some new boundary discretization techniques have been proposed and developed, such as singular boundary method (Gu et al., 2012, 2014; Gu et al., 2011) and Boundary Face Method (BFM) (Guo, et al., 2013; Huang, et al., 2012; Qin, et al., 2010; Zhang, et al., 2009; Zhou, et al., 2012). In order to avoid the error of geometry approximation, the BFM is employed in the numerical implementation, by which analyses can be performed directly on the CAD geometry model. The domain integrals which appear in the BIE are transformed into equivalent boundary integrals using the Dual Reciprocity Method (DRM) (Chen, et al., 2004; Partridge, et al., 1992). The 3D buckling equation is presented as a standard eigenvalue problem after introducing the boundary conditions and assembling the matrices. The eigenvalue problem yields the critical load factor and buckling modes as results.

In order to demonstrate the accuracy of the proposed formulation, some classical structures, such as plate, beam and rod, are modeled as 3D solid with different loadings and boundary conditions to be analyzed in the initial phase of the study. Results are compared with the finite element method (FEM) results and analytical results, and a good agreement is obtained. In the future work, it can be expected to apply this method to analyze the buckling of engineering structures with arbitrary shapes and features.

This paper is organized as follows: A completely new control equation for buckling analysis of 3D elastic solid is derived in Section 2. The corresponding BIE and the domain integral approaches are illustrated in Sections 3 and 4 respectively. In Section 5 we present the numerical implementation with BFM. Some numerical examples are presented in Section 6, and finally, the paper ends with conclusions in Section 7.

2 Governing equations

In this section, a new control equation will be derived. First of all, we will use the Principle of potential energy to get the equilibrium equations after deformation. The potential energy of the elastomer can be expressed as (Washizu, 1975)

$$\Pi=\iiint_V [U(e_{ij}) - f_i u_i]dV - \iint_{S_\sigma} \bar{p}_i u_i ds \tag{1}$$

where $U(e_{ij})$ is the strain energy density. f_i, u_i and p_i represent body force, displacement and traction respectively. e_{ij} is the Green strain tensor. According to the Principle of potential energy, the equilibrium equation should satisfy the following equation:

$$\delta\Pi=\iiint_V [\frac{\partial U(e_{ij})}{\partial e_{ij}} \delta e_{ij} - f_i \delta u_i]dV - \iint_{S_\sigma} \bar{p}_i \delta u_i ds = 0 \tag{2}$$

Because of the randomicity of the δu_i and the following constitutive relation of the elastomer,

$$\sigma_{ij} = \frac{\partial U(e_{ij})}{\partial e_{ij}} = d_{ijhl} e_{hl}, \quad (\Omega + \mathrm{S}) \tag{3}$$

we can get the equilibrium equations as follows:

$$\begin{cases} [(\delta_{ki} + u_{k,i})\sigma_{ij}]_{,j} + f_k = 0 & (\Omega) \\ (\delta_{ki} + u_{k,i})\sigma_{ij} n_k - \bar{p}_k = 0, & (S_\sigma) \end{cases} \tag{4}$$

where n_k is the Cosine of the angle between the normal of the boundary and coordinate axis. δ_{ki} is the Kronecker delta function.

In order to finding the critical state from pre-buckling state to buckling state, we should investigate the higher-order derivation of the potential energy mentioned before.

$$\begin{aligned} \delta^2\Pi &= -\iiint_V \delta\{[(\delta_{ki} + u_{k,i})\sigma_{ij}]_{,j}\}\delta u_k dV + \iint_{S_\sigma} \delta\{(\delta_{ki} + u_{k,i})\sigma_{ij} n_j\}\delta u_k ds \\ &= -\iiint_V \{\sigma_{ij}\delta u_{k,i} + (\delta_{ki} + u_{k,i})\delta\sigma_{ij}\}_{,j}\delta u_k dV + \iint_{S_\sigma} \{\sigma_{ij}\delta u_{k,i} + (\delta_{ki} + u_{k,i})\delta\sigma_{ij}\} n_j \delta u_k ds \\ &= -\iiint_V \{\sigma_{ij}\delta u_{k,i} + (\delta_{ki} + u_{k,i}) d_{ijhl}(\delta_{mh} + u_{m,h})\delta u_{m,l}\}_{,j}\delta u_k dV \\ &\quad + \iint_{S_\sigma} \{\sigma_{ij}\delta u_{k,i} + (\delta_{ki} + u_{k,i}) d_{ijhl}(\delta_{mh} + u_{m,h})\delta u_{m,l}\} n_j \delta u_k ds \end{aligned} \tag{5}$$

If $\delta^2\Pi=0$, we can get the equation of the critical buckling state. Because of the randomicity of δu_k, the buckling equation of arbitrary infinitesimal can be expressed as:

$$\{\sigma_{ij}\delta u_{k,i} + (\delta_{ki} + u_{k,i}) d_{ijhl}(\delta_{mh} + u_{m,h})\delta u_{m,l}\}_{,j} = 0 \tag{6}$$

where σ_{ij} and u_k are stress and displacement of the pre-buckling state respectively. Generally, the deformation in pre-buckling state is small and it can be obtained by linear-elastic analysis. Considering the constitutive relation, Eq. (3) can be re-expressed as:

$$\delta\sigma_{ij} = d_{ijhl}\delta e_{hl} = d_{ijhl}(\delta_{mh} + u_{m,h})\delta u_{m,l} \tag{7}$$

Insert Eq. (7) into Eq. (6), we can get:

$$\{\sigma_{ij}\delta u_{k,i} + (\delta_{ki} + u_{k,i})\delta\sigma_{ij}\}_{,j} = 0 \tag{8}$$

In the following part of this paper, we will note σ_{ij}, u_k in pre-buckling state as $\sigma_{ij}^{(0)}, u_k^{(0)}$. Based on the small deformation theory, we can assume that $u_{k,i}^{(0)} \ll 1$. And the Eq. (8) can be rewritten as

$$[\delta u_{k,i}\sigma_{ij}^{(0)} + \delta\sigma_{kj}]_{,j} = 0 \tag{9}$$

The following linear elastic Generalized Hook's Law was chosen as the constitutive relation.

$$d_{ijhl} = 2G\delta_{ih}\delta_{jl} + \lambda\delta_{ij}\delta_{hl} \tag{10}$$

where G is the Shear modulus and λ is the Lame parameter.

The variations $\delta u_{k,i}$ and $\delta\sigma_{ij}$, which are unknown, can be considered as the incremental from the pre-buckling state $\sigma_{ij}^{(0)}, u_k^{(0)}$ to buckling state $\sigma_{ij}^{(1)}, u_k^{(1)}$. We note $\delta u_{k,i}$, $\delta\sigma_{ij}$ directly as $u_{k,i}$, σ_{ij}. And the displacement and stress in buckling can be noted as $\bar{p}\cdot u_{k,i}$, $\bar{p}\cdot\sigma_{ij}$, where $\bar{p}$ is a factor loading. Considering the Eq. (10), the Eq. (9) can be reformed into the following expression:

$$\bar{p}\bar{\sigma}_{ij}^{(0)}u_{k,ij} + (Gu_{k,jj} + (G+\lambda)u_{j,jk}) = 0 \tag{11}$$

This is a new linearly differential equation of buckling anaysis. Compared with the classical theory, this equation considers the displacement in three directions. It can be used to analyze the buckling problem of 3D solid with arbitrary shape.

3 Boundary integral equation

The Kelvin fundamental solutions of displacement and traction are employed to be the fundamental solutions of the Eq. (11)

$$\begin{aligned} u_j^*(x) &= U_{ij}^*(\xi, x)e_i(\xi) \\ p_j^*(x) &= P_{ij}^*(\xi, x)e_i(\xi) \end{aligned} \tag{12}$$

in which

$$\begin{aligned} U_{ij}^*(\xi, x) &= \frac{1}{16\pi(1-\mu)Gr}\{(3-4\mu)\delta_{ij} + r_{,i}r_{,j}\} \\ P_{ij}^*(\xi, x) &= \frac{-1}{8\pi(1-\mu)r^2}\{[(1-2\mu)\delta_{ij} + 3r_{,i}r_{,j}]\frac{\partial r}{\partial n} - (1-2\mu)(r_{,i}n_j - r_{,j}n_i)\} \end{aligned} \tag{13}$$

where $U_{ij}^*(\xi, x)$ and $P_{ij}^*(\xi, x)$ present the displacements and tractions in the j direction at point x corresponding to a unit force acting in the i direction applied at point ξ. The fundamental solutions in Eq. (12) satisfy the following function

$$Gu^*_{k,jj} + (G+\lambda)u^*_{j,jk} = -\delta(\xi, x)e_k(\xi) \tag{14}$$

Using the Betti's reciprocal theorem, Eq. (11) can be converted into the following equation:

$$\begin{aligned} &u_k(\xi)\delta_{ki}e_i(\xi) + \int_\Gamma P_{ik}^*(\xi, x)e_i(\xi)u_k(x)d\Gamma(x) \\ &= \bar{p}\int_\Omega \bar{\sigma}_{ij}^{(0)}u_{k,ij}U_{ik}^*(\xi, x)e_i(\xi)d\Omega(x) + \int_\Gamma p_k(x)U_{ik}^*(\xi, x)e_i(\xi)d\Gamma(x) \end{aligned} \tag{15}$$

Taking the point ξ in Eq. (15) to the boundary and accounting for the jump of the left-hand side integral yields the BIE:

$$
\begin{aligned}
&c_{ik}(\xi)u_k(\xi)+\int_\Gamma P_{ik}^*(\xi,x)u_k(x)d\Gamma(x)\\
&=\int_\Gamma U_{ik}^*(\xi,x)\,p_k(x)d\Gamma(x)+\bar{p}\int_\Omega U_{ik}^*(\xi,x)\bar{\sigma}_{mn}^{(0)}u_{k,mn}d\Omega(x)
\end{aligned}
\tag{16}
$$

where $c_{ik}(\xi)=0.5\delta_{ik}$ when ξ is located on smooth surfaces. For the domain integral in Eq. (16), we should transform it into boundary integral to retain the dimension reduction advantage of BEM, which will be discussed in the next section.

4 Boundary transformation of domain integral

Firstly, we note the domain integral as:

$$
D=\int_\Omega U_{ik}^*(\xi,x)b_k(x)d\Omega(x)=\int_\Omega U_{ik}^*(\xi,x)\bar{\sigma}_{mn}^{(0)}u_{k,mn}d\Omega(x) \tag{17}
$$

in which

$$
b_k(x)=\bar{\sigma}_{mn}^{(0)}u_{k,mn}(x) \tag{18}
$$

Then, the following approximation for $b_k(x)$ is proposed:

$$
b_j=\sum_{k=1}^{N+L}a_j^k f^k(r) \qquad \text{or} \qquad \mathbf{b=F\alpha} \tag{19}
$$

where the α_j are a set of initially unknown coefficients and f^k are approximating function which have the following particular solution

$$
\nabla^2\hat{u}_j^k=f^k \tag{20}
$$

Then, using the DRM (Partridge, et al., 1992), the domain integral can be transformed into boundary and the Eq. (16) can be expressed as:

$$
\begin{aligned}
&c_{ij}(\xi)u_j(\xi)+\int_\Gamma P_{ij}^*(\xi,x)u_j(x)d\Gamma(x)-\int_\Gamma U_{ij}^*(\xi,x)\,p_j(x)d\Gamma(x)\\
&=\bar{p}\sum_{k=1}^{N+L}\alpha_l^k\left\{c_{ij}(\xi)\hat{u}_{jl}^k(\xi)+\int_\Gamma P_{ij}^*(\xi,x)\hat{u}_{jl}^k(x)d\Gamma(x)-\int_\Gamma U_{ij}^*(\xi,x)\hat{q}_{jl}^k(x)d\Gamma(x)\right\}
\end{aligned}
\tag{21}
$$

After discretization and approximation of the variation of *u*, *p* over each element using their nodal values and the same set of interpolation functions, Eq. (21) becomes

$$
\begin{aligned}
&c_{ij}(\xi)u_j(\xi)+\sum_{m=1}^{M}\int_{\Gamma_m}P_{ij}^*(\xi,x)\cdot\left(\sum_{n=1}^{Np}N_n(x)\cdot u_j(x_n)\right)d\Gamma(x)-\sum_{m=1}^{M}\int_{\Gamma_m}U_{ij}^*(\xi,x)\cdot\left(\sum_{n=1}^{Np}N_n(x)\cdot p_j(x_k)\right)d\Gamma(x)\\
&=\bar{p}\sum_{k=1}^{N+L}\alpha_l^k\left\{c_{ij}(\xi)\hat{u}_{jl}^k(\xi)+\sum_{m=1}^{M}\int_{\Gamma_m}P_{ij}^*(\xi,x)\cdot\left(\sum_{n=1}^{Np}N_n(x)\cdot\hat{u}_{jl}^k(x_n)\right)d\Gamma(x)-\sum_{m=1}^{M}\int_{\Gamma_m}U_{ij}^*(\xi,x)\left(\sum_{n=1}^{Np}N_n(x)\cdot\hat{q}_{jl}^k(x_n)\right)d\Gamma(x)\right\}
\end{aligned}
\tag{22}
$$

where *Np* is the number of interpolation points in an boundary element. It should be mentioned that the BFM is implemented directly based on the boundary representation data structure (B-rep) that is used in most CAD packages for geometry modeling. Each bounding surface of geometry model is represented as parametric form by the geometric map between the parametric space and the physical space. Both boundary integration and variable approximation are performed in the parametric space. The integrand quantities are calculated directly from the faces rather than from elements, and thus no geometric error will be introduced. The scheme for calculating nearly singular integral is of great importance to BIE based method to analyzed thin structure (Atluri et al, 2003, 2004, 2006; Liu, 1998; Qin, 1993; Xie et al, 2013). The scheme we applied in this paper is

the subdivision scheme. The main idea of this scheme is employing more integral points to calculate the integral over the boundary patches near the source points. For more details of the implementation, refer to (Zhang, et al., 2009).

Finally, applying the above equation to all boundary nodes, the following system

$$\mathbf{Hu - Gp} = \bar{\mathrm{p}}\mathbf{(H\hat{u} - G\hat{p})\alpha} \tag{23}$$

can be obtained, in which $\boldsymbol{\alpha} = (\mathbf{F}^{-1}\boldsymbol{\sigma}\mathbf{F}''\mathbf{F}^{-1})\mathbf{u}$. So the above equation can be reformed into

$$\mathbf{Hu - Gp} = \bar{\mathrm{p}}\mathbf{(H\hat{u} - G\hat{p})}(\mathbf{F}^{-1}\boldsymbol{\sigma}\mathbf{F}''\mathbf{F}^{-1})\mathbf{u} \tag{24}$$

In this equation, only boundary integration is included, the numerical calculation of it will be discussed in the next section.

5 Numerical implementation

In this section, the numerical procedure for solving the Eq. (24) is presented. The first step is to solve the BIE of linear elasticity problem and calculate the stress results of the nodes. Next the BIE of buckling problem is solved.

5.1 Boundary conditions

Firstly, the boundary conditions in each stage of buckling analysis are discussed. In pre-buckling state, the boundary conditions can be expressed as

$$\begin{cases} u_i^{(0)} = \bar{u}_i^{(0)}(x), & x \in S_u \\ p_i^{(0)} = \bar{p}_i^{(0)}(x), & x \in S_\sigma \end{cases} \tag{25}$$

where x is the coordination of the initial configuration. Generally, the boundary condition type will not change going with the deformation. But the value of them may become the following expression:

$$\begin{cases} u_i^{(1)} = \bar{u}_i^{(1)}(\xi), & \xi \in S_u \\ p_i^{(1)} = \bar{p}_i^{(1)}(\xi), & \xi \in S_\sigma \end{cases} \tag{26}$$

where ξ is the coordination in buckling state. Subtracting Eq. (25) from Eq. (26), the boundary condition in incremental form can be expressed as

$$\begin{cases} u_i = \bar{u}_i(\xi), & x \in S_u \\ p_i = \bar{p}_i(\xi), & x \in S_\sigma \end{cases} \tag{27}$$

where u_i and p_i are the displacement and traction increment.

If we assume that the load and the constraint are conservational, which means that the value of them will not change before and after buckling, the values of the increments will be equal to zero.

$$\begin{cases} u_i = 0, & x \in S_u \\ p_i = 0, & x \in S_\sigma \end{cases} \tag{28}$$

In this paper, only the state when the boundary conditions are conservational is discussed.

5.2 Buckling analysis

In the first stage, we have to solve an elasticity problem with the boundary conditions in Eq. (25).

And the following equation should be solved.

$$Gu_{k,jj} + (G+\lambda)u_{j,jk} = 0 \tag{29}$$

And the results of it will be used in the next stage.

In the second stage, Eq. (23) will be solved. Considering the models what we study are all thin, we only employ the boundary nodes to interpolate the domain functions in DRM. Because it is near between the upper and lower surfaces, high precision will still be obtained without using domain nodes for interpolation. Therefore all the unknowns are on the boundary and no additional matrix need to be computed. Considering Eq. (24), we denote

$$\mathbf{S} = (\mathbf{H}\hat{\mathbf{u}} - \mathbf{G}\hat{\mathbf{p}})(\mathbf{F}^{-1}\boldsymbol{\sigma}\mathbf{F}''\mathbf{F}^{-1}) \tag{30}$$

And Eq. (24) can be rewritten as

$$\mathbf{Hu} - \mathbf{Gp} = \bar{\mathrm{p}}\mathbf{Su} \tag{31}$$

Considering the boundary conditions in Eq. (28) and denote $u=u_1$ when x on S_u and $q=q_1$ when x on S_σ, the above equation can be rewritten using submatrices as

$$\begin{bmatrix} \mathbf{H}_{11} & \mathbf{H}_{12} \\ \mathbf{H}_{21} & \mathbf{H}_{22} \end{bmatrix} \begin{Bmatrix} u_1 \\ u \end{Bmatrix} - \begin{bmatrix} \mathbf{G}_{11} & \mathbf{G}_{12} \\ \mathbf{G}_{21} & \mathbf{G}_{22} \end{bmatrix} \begin{Bmatrix} p \\ p_2 \end{Bmatrix} = \bar{\mathrm{p}} \begin{bmatrix} \mathbf{S}_{11} & \mathbf{S}_{12} \\ \mathbf{S}_{21} & \mathbf{S}_{22} \end{bmatrix} \begin{Bmatrix} 0 \\ u \end{Bmatrix} \tag{32}$$

where $\mathbf{G}_{11}$ is a square matrix whose order is the same as the number of the nodes on S_σ. Taking into account that $u_1=0$ and $p_2=0$, we get

$$\begin{aligned} \mathbf{H}_{12}\mathbf{u} - \mathbf{G}_{11}\mathbf{p} &= \bar{\mathrm{p}}\mathbf{S}_{12}\mathbf{u} \\ \mathbf{H}_{22}\mathbf{u} - \mathbf{G}_{21}\mathbf{p} &= \bar{\mathrm{p}}\mathbf{S}_{22}\mathbf{u} \end{aligned} \tag{33}$$

Eliminating **p** between the above two equations in Eq. (33) gives

$$\left(\mathbf{H}_{22} - \mathbf{G}_{21}\mathbf{G}_{11}^{-1}\mathbf{H}_{12}\right)\mathbf{u} = \bar{\mathrm{p}}\left(\mathbf{S}_{22} - \mathbf{G}_{21}\mathbf{G}_{11}^{-1}\mathbf{S}_{12}\right)\mathbf{u} \tag{34}$$

or

$$\mathbf{Ku} = \bar{\mathrm{p}}\mathbf{Mu} \tag{35}$$

where

$$\begin{aligned} \mathbf{K} &= \mathbf{H}_{22} - \mathbf{G}_{21}\mathbf{G}_{11}^{-1}\mathbf{H}_{12} \\ \mathbf{M} &= \mathbf{S}_{22} - \mathbf{G}_{21}\mathbf{G}_{11}^{-1}\mathbf{S}_{12} \end{aligned} \tag{36}$$

Eq. (35) represents an equation of generalized algebraic eigenvalue/eigenvector problem. If we denote

$$\mathbf{Au} = \bar{\lambda}\mathbf{u} \tag{37}$$

where $\mathbf{A} = \mathbf{K}^{-1}\mathbf{M}$ and $\bar{\lambda} = \dfrac{1}{\bar{\mathrm{p}}}$. The solutions of Eq. (35) can be obtained directly by QR decomposition.

6 Numerical examples

Several numerical examples are presented to demonstrate the accuracy of the proposed method. Buckling problems with different geometries, loadings and boundary conditions are analyzed. The results are compared with analytical results and finite element results. In the following examples, the elastic modulus *E=1.0e11* and the Poisson's ratio *v=0.25* are adopted as material properties. The multiquadric radial basis function (RBF) is employed in the DRM. All of the models are

discretized with partially continuous elements, which are discontinuous at the edge of a face but continuous inside the face, in order to treat the corners of a body surfaces in a simple manner while not to generate too many nodes.

6.1 Example 1: Buckling of plate with dimensions of a:b:h=200:200:2

In the first example, we consider a plate with dimensions of *a=200, b=200* and *h=2* as shown in Fig. 1. The boundary conditions are shown in this figure as: The left and right surfaces of the plate are under loadings *q*=1000 along the *x* direction, while the other two directions of them are constrained. The front and back surfaces are constrained in *z* direction. The other surfaces are free. We discretize the model with 1010 nodes, quadratic quadrilateral elements are used on the upper and lower surfaces and the constant elements are used on the other four side surfaces as shown in Fig. 2.

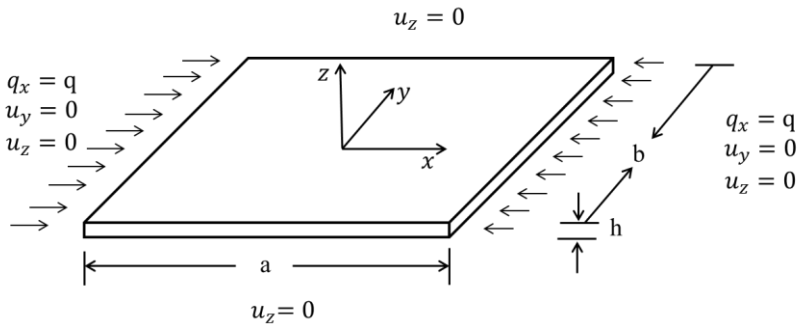

Figure 1: Geometry and loading of plate buckling model.

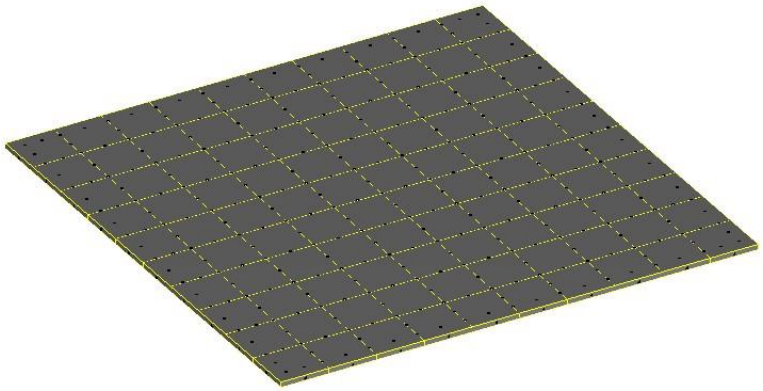

Figure 2: The discretized model of plate.

We plot the contours of results in three directions respectively as shown in Fig. 3 to Fig. 5, and present the mode shape of the first order in Fig. 6. From these figures, it can be seen that the results are in accordance with that of FEM.

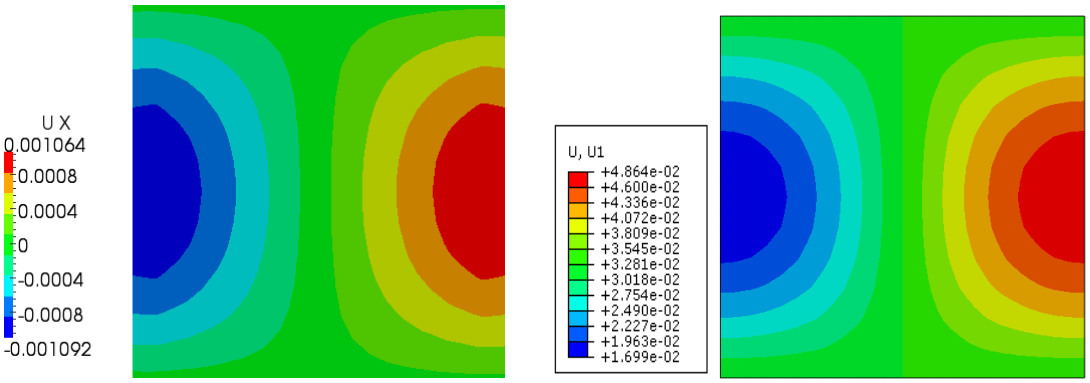

(a) Contour plot of BFM. (b) Contour plot of FEM.

Figure 3: Displacements in *x* direction.

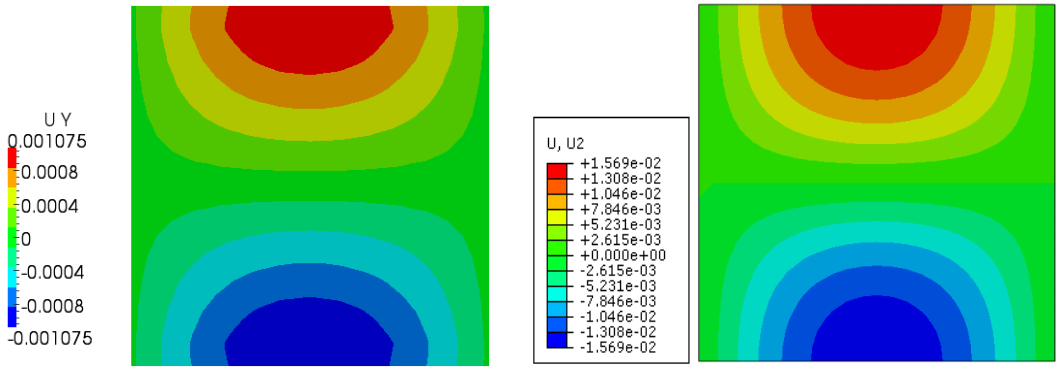

(a) Contour plot of BFM. (b) Contour plot of FEM.

Figure 4: Displacements in *y* direction.

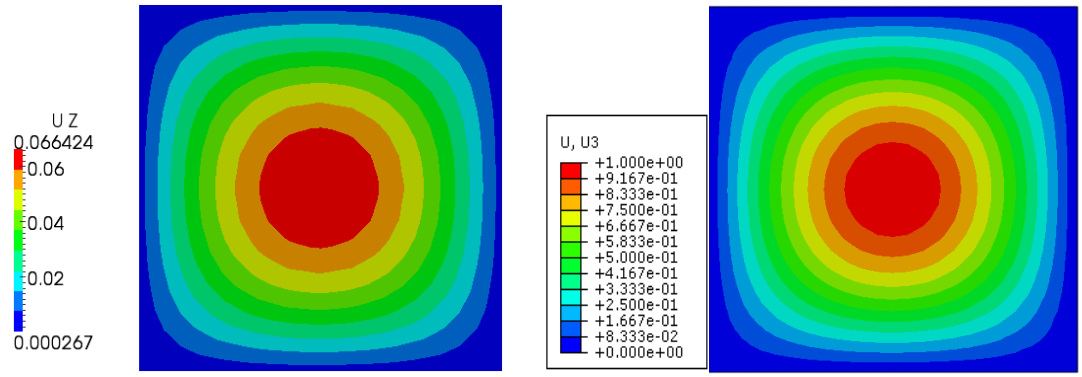

(a) Contour plot of BFM. (b) Contour plot of FEM.

Figure 5: Displacements in *z* direction.

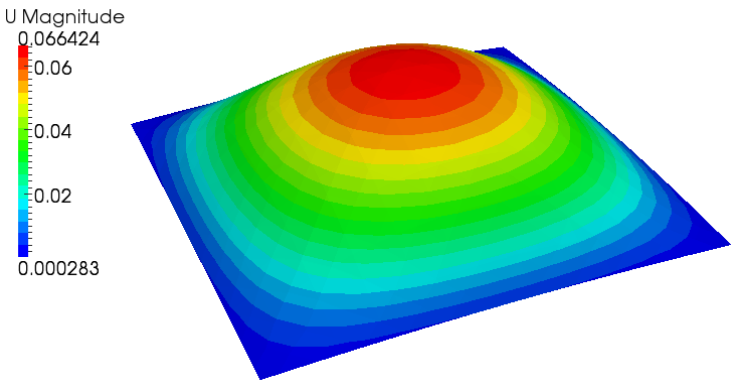

(a) The first order mode shape of BFM.

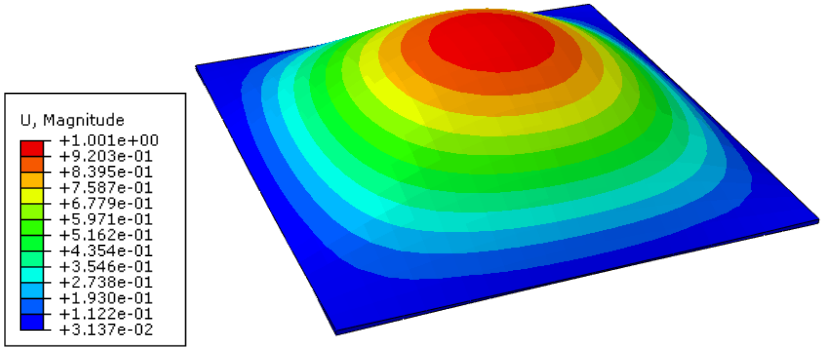

(b) The first order mode shape of FEM.

Figure 6: The first order mode shape of plate buckling.

The analytical solution of critical load can be found in reference (Brush and Almorth, 1975) and is given as

$$p_{cr} = k\frac{\pi^2 D}{Ab^2} \tag{38}$$

where $k = \left(\frac{b}{a}+\frac{a}{b}\right)^2$, $D = \frac{h^3 E}{12(1-\nu^2)}$, $A = bh$. A comparison of the results of BFM, FEM and analytical solution is illustrated in the last column of Table 1, a good agreement can be observed.

Table 1: The comparison of critical loads in example 1

Method	Number of nodes	Critical load
BFM	1010	3.5874E7
FEM	1131	3.3412E7
Classical theory		3.5092E7

6.2 Example 2. Buckling of plates with dimensions of a:b:h=400:200:2

In this example, we discuss the buckling of plate with dimensions of *a=400, b=200, h=2*. The boundary conditions are the same as that in example 1. The first order mode shape is compared with that obtained by FEM in Fig. 7, good agreements can be observed. Number of the discretized nodes used in BFM and FEM are listed in the third column of Table 2, and the results of critical

loads of them are illustrated in the last column. From Table 2, it can be found that a similar value of the critical load can be obtained with fewer nodes in our method compared with FEM.

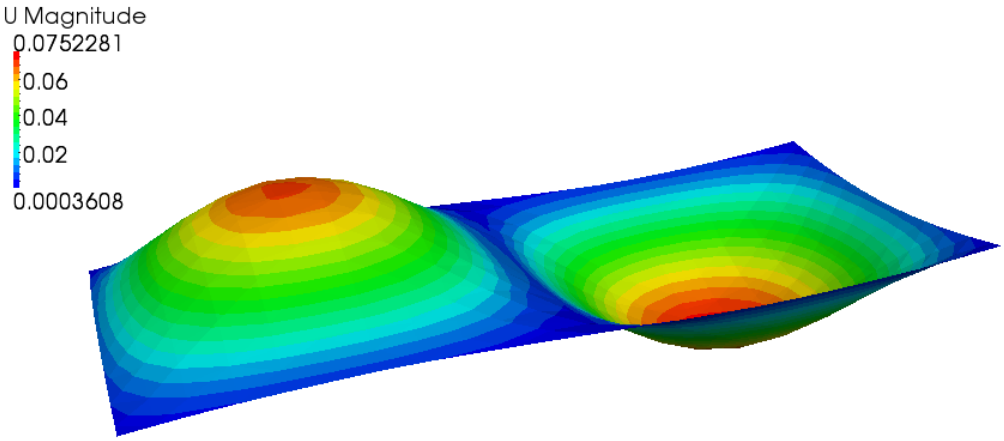

(a) The first order mode shape of BFM.

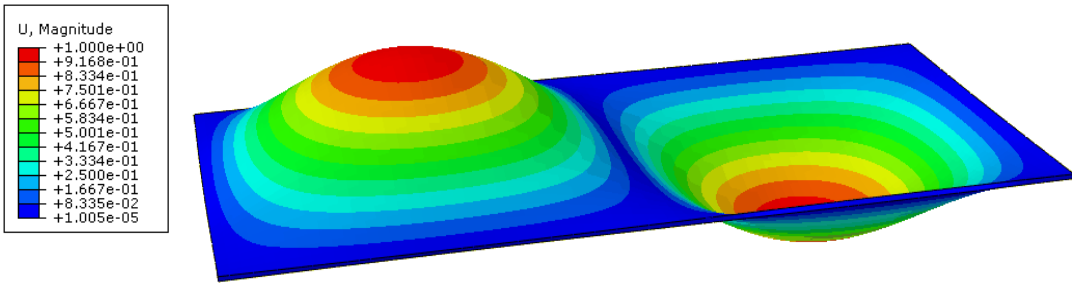

(b) The first order mode shape of FEM.

Figure 7: The first order mode shape of the plate with a:b:h=400:200:2.

Table 2: The comparison of critical loads of plate in example 2

Dimensions of plate	Method	Number of nodes	Critical load
a:b:h=400:200:2	BFM	592	3.4693E7
	FEM	1553	3.4126E7

6.3 Example 3. Buckling of beam with dimensions of l:a=100:2

In this example, a rectangular beam as shown in Fig. 8 is analyzed. The geometry and boundary conditions are shown in this figure. The right end surface of the beam is under loading q=100 along the z direction, while the other two directions of this surface are constrained. The left end surface of the beam is fixed in three directions. The other surfaces are free. The two square surfaces at both ends are discretized with four constant elements and quadratic quadrilateral elements are used to discretize the other four surfaces.

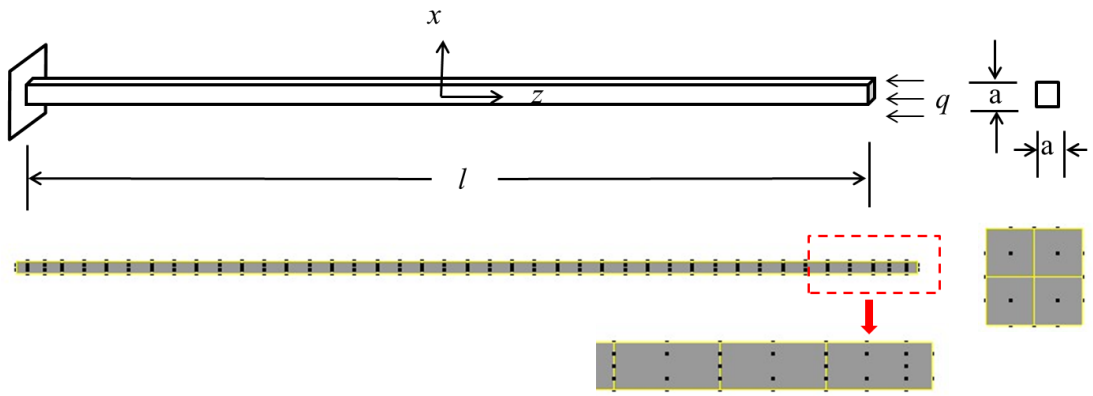

Figure 8: The geometry and the discretized model of the beam.

The mode shapes of the first order to the third order are presented in Fig. 9 to Fig. 11 respectively. The results of FEM are also shown in these figures. From them, it can be seen that the results are totally in accordance with that of FEM.

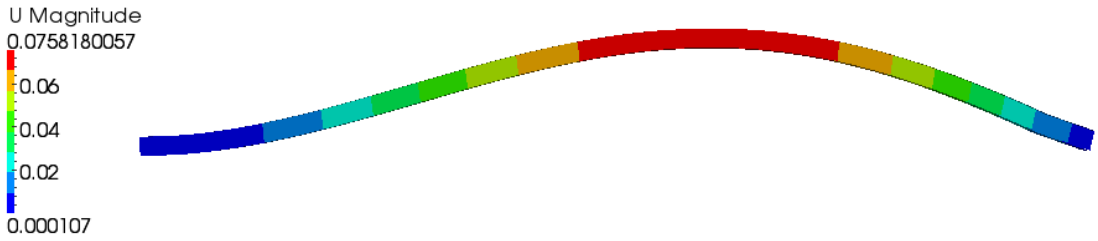

(a) The first order mode shape of BFM.

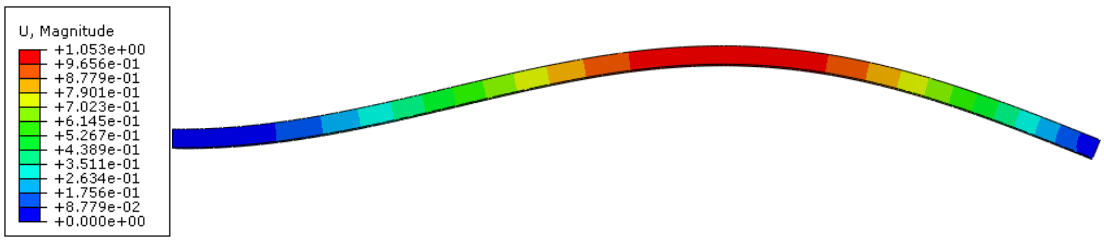

(b) The first order mode shape of FEM.

Figure 9: The first order mode shape of beam buckling.

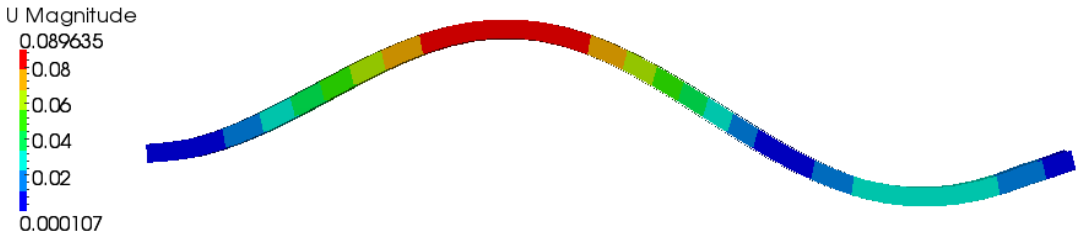

(a) The second order mode shape of BFM.

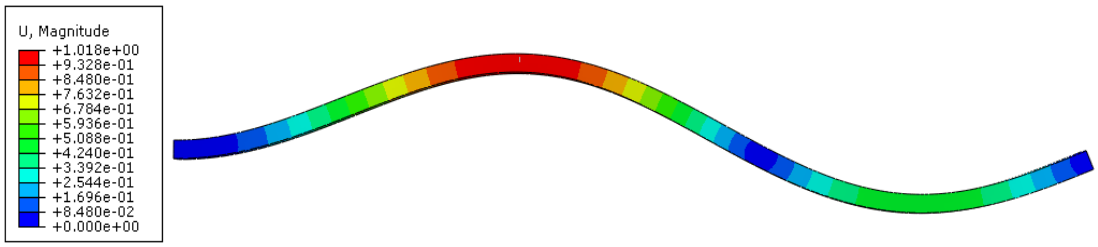

(b) The second order mode shape of FEM.

Figure 10: The second order mode shape of beam buckling.

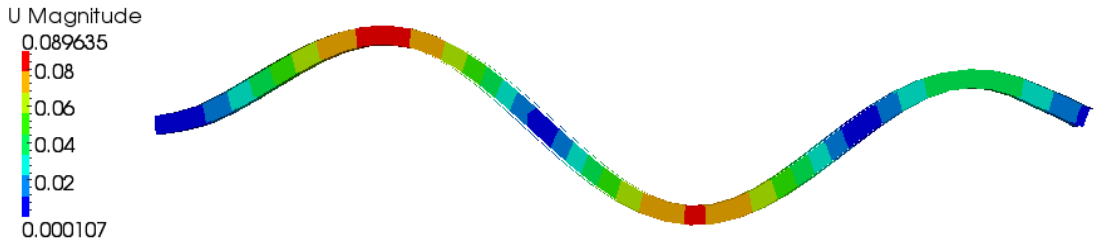

(a) The third order mode shape of BFM.

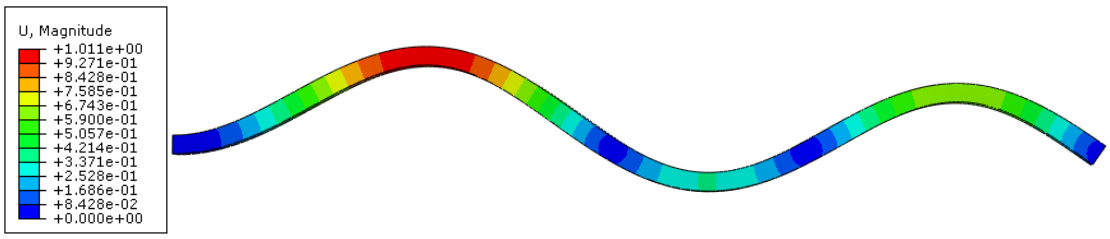

(b) The third order mode shape of FEM.

Figure 11: The third order mode shape of beam buckling.

Eq. (39) shows the formula of the analytical solution of critical load

$$p_{cr} = \frac{\pi^2 EI}{A(\mu l)^2} \tag{39}$$

where $\mu=0.7$, $I = a^4/12$ and $A = a^2$. The number of nodes and the values of critical loads obtained by BFM, FEM and the analytical method are illustrated in Table 3. For our method, much less nodes are required.

Table 3: The comparison of critical loads of beam

Method	Number of nodes	Critical load
BFM	460	6.62302E7
FEM	3021	6.71298E7
Classical theory		6.71404E7

6.4 Example 4. Buckling of rod with dimensions of l:r=100:1

In the last example, a rod with circle cross section is considered. It is subjected to a compression load in the *z* direction *q=100*. Eq. (39) shows the formula of the analytical solution when $\mu=0.7$, $I = (\pi r^4)/4$ and $A = \pi r^2$. The boundary conditions are the same as that of the beam in example

3. The geometry and the discretized model are shown in Fig. 12.

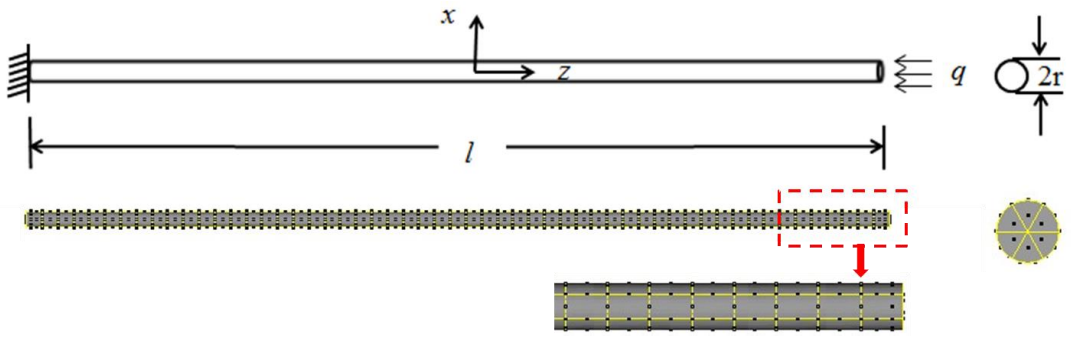

Figure 12: Geometry and the discretized model of rod.

Similarly, we plot the mode shapes of the first order to the third order in Fig. 13 to Fig. 15 respectively. The results are in accordance with that of FEM, the accuracy of the proposed method is verified again.

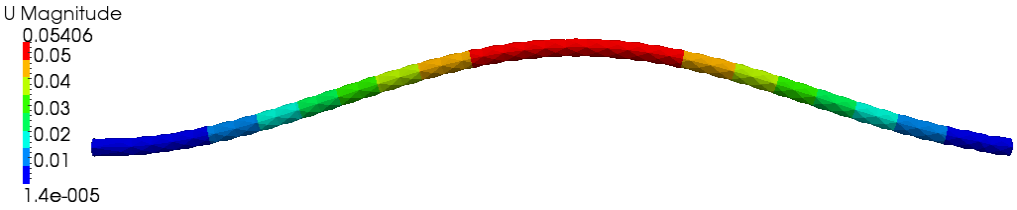

(a) The first order mode shape of BFM.

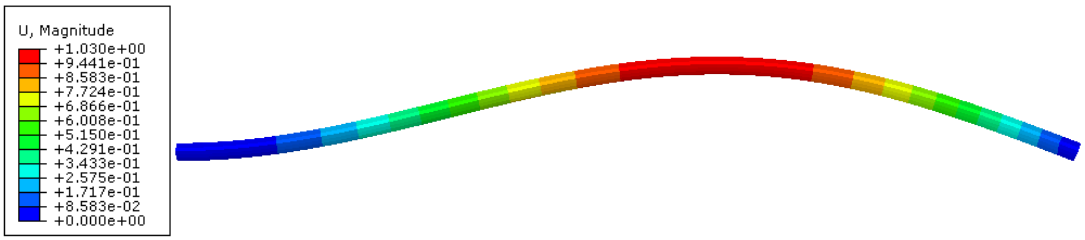

(b) The first order mode shape of FEM.

Figure 13: The first order mode shape of rod buckling.

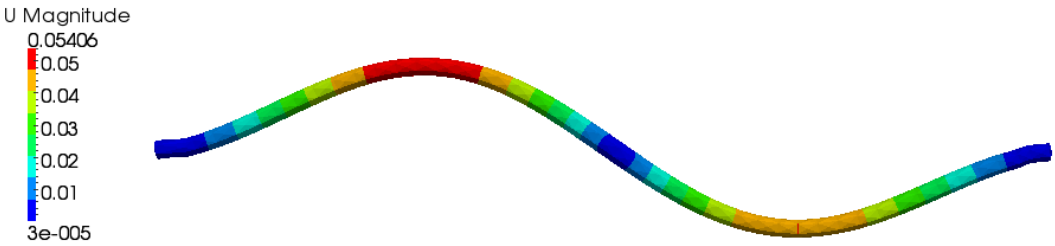

(a) The second order mode shape of BFM.

(b) The second order mode shape of FEM.

Figure 14: The second order mode shape of rod buckling.

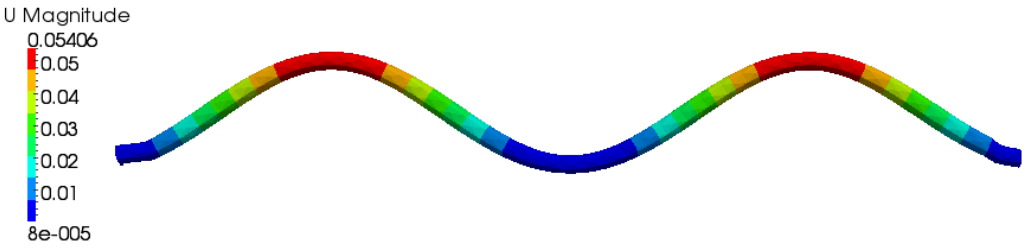

(a) The third order mode shape of BFM.

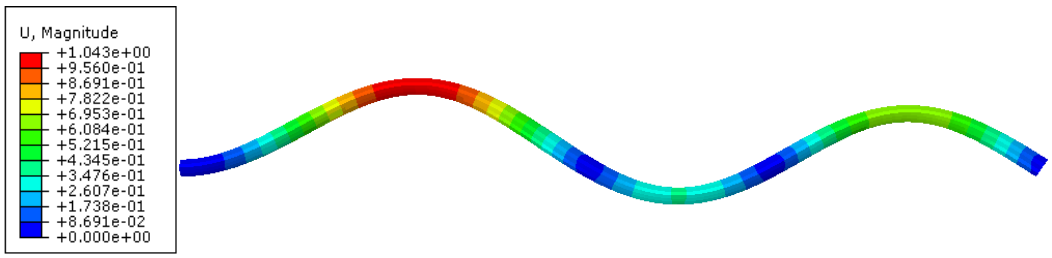

(b) The third order mode shape of FEM.

Figure 15: The third order mode shape of rod buckling.

We list the number of nodes used in BFM and FEM in the second column of Table 4. From the last column of Table 4, it can be seen that the value of the critical load obtained by BFM is smaller than the FEM solution and analytical solution. Actually the experimental result is always 65%~75% of the analytical solution in the rod buckling, and our results are more consistent with the experimental results than FEM.

Table 4: The comparison of critical loads of rod

Method	Number of nodes	Critical load
BFM	925	4.70382E7
FEM	3021	5.05577E7
Classical theory		5.03551E7

7 Conclusions

In this paper, a new concept, namely the Complete Solid Buckling Analysis, is proposed. This method makes it possible for us to solve the stability problems of the real engineering structures. The innovations of the proposed method and the conclusions can be summarized as follows:

1) Discarding the deformation assumptions for rods, beams, plates or shells, we derived a completely new control equation for 3D solid buckling problems based on the Principle of potential energy. In this equation, the displacements in three directions are considered.

2) In the numerical implementation of solving BIE, the BFM is adopted to avoid the errors of geometry approximation, and the DRM is employed to deal with the domain integrals.

3) Several examples of plate, beam and rod buckling analyses with different boundary conditions are investigated to test the accuracy of the proposed method. The mode shapes of the first three orders of buckling results are plotted and compared with that obtained by FEM, they are in good agreements. The critical loads are also compared with the results of FEM or the analytical solution, high accuracy is observed.

4) We can expect that higher accurate solutions of the control equation will be obtained if we use another more stable method to evaluate the domain integrals, e.g. direct integration using domain cells, and perfect the implementation of boundary integration in our program. Nevertheless, this is a novel and inspiring method for buckling analysis which is worth to give a further study.

Acknowledgements: This work was supported in part by the Key Project of National Science Foundation of China (NSFC) under grant number 61232014, in part by National 973 Project of China under grant number 2010CB328005, in part by National Science Foundation of China under grant number 11172098, in part by Hunan Provincial Innovation Foundation for Postgraduate under grant number CX2013B150.

References

Aliabadi, M.H. (2001): The boundary element method, Application to solids and structures, vol. 2. Chichester, Wiley.

Atluri, S.N.; Han, Z.D.; Shen, S. (2003): Meshless Local Petrov-Galerkin (MLPG) approaches for weakly-singular traction & displacement boundary integral equations. *CMES-Comput. Model. Eng. Sci.*, vol. 4, no. 5, pp. 507-517.

Atluri, S.N. (2004): The Meshless Local Petrov-Galerkin (MLPG) Method for Domain & Boundary Discretizations, Tech Science Press, 665 pages.

Atluri, S.N.; Liu, H.T.; Han, Z.D. (2006a): Meshless Local Petrov-Galerkin (MLPG) Mixed Collocation Method for Elasticity Problems. *CMES-Comput. Model. Eng. Sci.*, vol. 14, no. 3, pp. 141-152.

Atluri, S.N.; Liu, H.T.; Han, Z.D. (2006b): Meshless Local Petrov-Galerkin (MLPG) Mixed Finite Difference Method for Solid Mechanics. *CMES-Comput. Model. Eng. Sci.*, vol. 15, no. 1, pp. 1-16.

Baiz, P.M.; Aliabadi, M.H. (2006): Linear buckling analysis of shear deformable shallow shells by the boundary domain element method. *CMES-Comput. Model. Eng. Sci*., vol. 13, no. 1, pp. 19-34.

Baiz, P.M.; Aliabadi, M.H. (2007): Buckling analysis of shear deformable shallow shells by the boundary element method. *Eng. Anal. Bound. Elem*., vol. 31, no. 4, pp. 361-372.

Brebbia, C.A. (1978): The Boundary Element Method for Engineers, Pentech Press, London.

Cheng, A.H.D.; Cheng, D.T. (2005): Heritage and early history of the boundary element method.

Eng. Anal. Bound. Elem., 29, 268-302.

Brush, D.O.; Almorth, B.O. (1975): Buckling of Bars, Plates and Shells. McGraw-Hill, New York.

Chen, J.T.; Chen, I.L.; Chen, K.H.; Yeh, Y.T.; Lee, Y.T. (2004): A meshless method for free vibration of arbitrarily shaped plates with clamped boundaries using radial basis function. *Eng. Anal. Bound. Elem.*, vol. 5, pp. 535-545.

Gu, Y.; Chen, W.; He, X.Q. (2012): Singular boundary method for steady-state heat conduction in three dimensional general anisotropic media. *Int. J. Heat Mass Transf.*, Vol. 55, No. 17–18, pp. 4837-4848.

Gu, Y.; Chen, W.; He, X.Q. (2014) Improved singular boundary method for elasticity problems. *Comput. Struct.*, Vol. 135, No. 0, pp. 73-82.

Gu, Y.; Chen, W.; Zhang, C.Z. (2011): Singular boundary method for solving plane strain elastostatic problems. *Int. J. Solids Struct.*, vol. 48, No. 18, pp. 2549-2556.

Guo, S.P.; Zhang, J.M.; Li, G.Y.; Zhou, F.L. (2013): Three-dimensional transient heat conduction analysis by Laplace transformation and multiple reciprocity boundary face method. *Eng. Anal. Bound. Elem.*, vol. 37, pp. 15-22.

Huang, C.; Zhang, J.M.; Qin, X.Y.; Lu, C.J.; Sheng, X.M.; Li, G.Y. (2012): Stress analysis of solids with open-ended tubular holes by BFM. *Eng. Anal. Bound. Elem.*, vol. 36, pp. 1908-1916.

Lin, J.; Duffield, R.C.; Shih, H. (1999): Buckling analysis of elastic plates by boundary element method. *Eng. Anal. Bound. Elem.*, vol. 23, pp. 131-137.

Liu, Y.J. (1998): Analysis of shell-like structures by the boundary element method based on 3-D elasticity: formulation and verification. *Int. J. Numer. Meth. Eng.*, vol. 41, pp. 541-558.

Long, S.; Atluri, S.N. (2002): A meshless local Petrov-Galerkin method for solving the bending problem of a thin plate. *CMES-Comput. Model. Eng. Sci*., vol. 3, no.1, pp. 53-64.

Manolis, G.D.; Beskos, D.E.; Pineros, M.F. (1986): Beam and plate stability by boundary elements. *Comput. Struct.*, vol. 22, pp. 917-923.

Nerantzaki, M.S.; Katsikadelis, J.T. (1996): Buckling of plates with variable thickness—an analog equation solution. *Eng. Anal. Bound. Elem.*, vol. 18, pp. 149-154.

Partridge, P.W.; Brebbia, C.A.; Wrobel, L.C. (1992): The Dual Reciprocity Boundary Element Method. Southampton and Springer-Verlag, Berlin and New York.

Purbolaksono, J.; Aliabadi, M.H. (2005): Buckling analysis of shear deformable plates by the boundary element method. *Int. J. Numer. Meth. Eng.*, vol. 62, pp. 537-63.

Qin, X.Y.; Zhang, J.M.; Li, G.Y.; Sheng, X.M. (2010): An element implementation of the boundary face method for 3D potential problems. *Eng. Anal. Bound. Elem.*, vol. 34, pp. 934-943.

Qin, Q.H. (1993): Nonlinear analysis of Reissner plates on an elastic foundation by the BEM. *Int. J. Solids Struct.*, vol. 30, pp. 3101-3111.

Sapountzakis, E.J.; Dourakopoulos, J.A. (2008): Flexural-torsional buckling analysis of composite beams by BEM including shear deformation effect. *Mech. Res. Commun.*, vol. 35, no. 8, pp. 497-516.

Syngellakis, S.; Elzein, A. (1994): Plate buckling loads by the boundary element method. *Int. J. Numer. Meth. Eng.*, vol. 37, pp. 1763-1778.

Timoshenko, S.; Gere, J.M. (1961): Theory of Elastic Stability (2nd edn.). McGraw-Hill, New York.

Washizu, K. (1975): Variational methods in elasticity and plasticity, 2nd ed., Pergamon Press,

London.

Xie G.Z.; Zhang J.M.; Huang C.; Lu C.J.; Li G.Y. (2013): Calculation of Nearly Singular Boundary Element Integrals in Thin Structures Using an Improved Exponential Transformation. *CMES-Comput. Model. Eng. Sci.*, vol. 94, no. 2, pp. 139-157.

Zhang, J.M.; Qin, X.Y.; Han, X.; Li, G.Y. (2009): A boundary face method for potential problems in three dimensions. *Int. J. Numer. Meth. Eng.*, vol. 80, pp. 320-337.

Zhou, F.L.; Zhang, J.M.; Sheng, X.M.; Li, G.Y. (2012): A dual reciprocity boundary face method for 3D non-homogeneous elasticity problems. *Eng. Anal. Bound. Elem.*, vol. 36, pp. 1301-1310.